PCCP

Accepted Manuscript

ROYAL SOCIETY OF CHEMISTRY

www.rsc.org/pccp

ARTICLE TYPE www. rsc.org/xxxxxx | XXXXXXXX

Photodissociation of aniline N–H bond in clusters of different nature†

Viktoriya Poterya,[a] Dana Nachtigallová,*[b] Jozef Lengyel,[a] and Michal Fárník*[a]

Received Xth XXXXXXXXXX 20XX, Accepted Xth XXXXXXXXX 20XX
First published on the web Xth XXXXXXXXXX 2015
DOI: 10.1039/b000000x

We investigated the solvent effects on the N–H bond photodisociation dynamics of aniline ($PhNH_2$) in clusters using velocity map imaging (VMI). The VMI experiment was accompanied by a time-of-flight mass spectrometry after electron ionization to reveal the cluster nature. The H-fragment images were recorded at 243 nm in various expansion regimes corresponding to different species: isolated molecules; small $(PhNH_2)_N$, $N \leq 3$, clusters; larger $(PhNH_2)_N$, $N \geq 10$; small mixed $PhNH_2{\cdot}(H_2O)_N$, $N \leq 10$, clusters; and individual $PhNH_2$ molecules deposited on large $(H_2O)_N$, $\bar{N} = 430$. The H-fragment kinetic energy distributions exhibit fast fragments around 0.8 eV (A) assigned previously to a direct dissociation along a repulsive $\pi\sigma^*$ state potential, and slow statistical fragments peaking near 0.2 eV (B). In the aniline clusters the contribution of fast fragments (A) decreases relative to (B) with increasing the cluster size. Similar effect is observed when aniline is solvated with water molecules. The experimental data are interpreted with *ab initio* calculations. Cluster structures were calculated with both N–H bonds of an aniline molecule participating in hydrogen bonding, as well as the ones with free N–H bonds. The latter ones yield preferentially the fast fragments as the isolated molecule. For the N–H engaged in hydrogen bonding a barrier increased along the N–H coordinate on the dissociative $\pi\sigma^*$ state potential surface, and also the energy of $\pi\sigma^*/S_0$ conical intersection increased. Thus the fast dissociation channel was closed stabilizing the molecule in clusters. The population could be funnelled through other conical intersections into the hot ground state which decayed statistically, yielding the slow H-fragments.

1 Introduction

The photophysical behavior of heteroaromatic systems, incuding phenol, pyrrole, and aniline has been subject of numerous experimental and theoretical papers covered in recent reviews.[1,2] A special attention has been paid to the nonradiative relaxation mechanism which utilizes the dissociative $\pi\sigma^*$ channel with the σ^* orbital localized on the X–H bond (X = O, N). This channel has been suggested to provide an effective relaxation route via $\pi\sigma^*/S_0$ conical intersection (CI) leading either to X–H bond fission or to the original species in the ground state.[3]

In this work we concentrate on the N–H bond dissociation in aniline ($PhNH_2$) at 243 nm and investigate the photochemistry of aniline solvated in various clusters. Small heteroaromatic molecules represent essential building blocks of larger biomolecules and act as ultraviolet (UV) chromophores in these biomolecules. Therefore the investigations of photodissociation behavior of the small heteroaromatic molecules in the gas phase can contribute to the understanding of biomolecule photostability. Aniline, in particular, represents a model system for investigations of photochemistry in the purine derived DNA bases guanine and adenine.[2,4] Studying the photodissociation in clusters provides a molecular-level insight into the solvent effects, which is a step towards understanding these processes in bulk.

Several recent experimental and computational studies on aniline photodynamics were reported.[4–12] These studies concentrated mainly on the role of $^1\pi\sigma^*$ channel in the excited state dissociation dynamics. Similarly to phenol, in the vertical Franck-Condon (vFC) region this state is of Rydberg character and it is located energetically between the first and second bright singlet states of $\pi\pi^*$ character. Details on the aniline dissociation are still a subject of discussion, in particular, various scenarios of the $\pi\sigma^*$ state population were suggested as discussed below.

Nevertheless, all previously reported experimental studies agreed that the excited $S_3(2^1\pi\pi^*)$ state is populated at the wavelengths $\leq$240 nm.[4–8] At these energies, a fast dissociation is observed via the sequence $2^1\pi\pi^*/1^1\pi\pi^*$, $1^1\pi\pi^*/^1\pi\sigma^*$ and $^1\pi\sigma^*/S_0$ CIs. Recently, Sala et al. reported the existence of a three-state CI of $2^1\pi\pi^*$, $1^1\pi\pi^*$ and $1^1\pi\sigma^*$ states which can utilize the N-H bond fission,[13] and these theoretical calculations have been also confirmed experimentally.[12] The corresponding CIs can occur also in the out-of-plane coordinates of a complex potential energy surface which can be found in Fig. 3 of Ref.[4].

† Electronic Supplementary Information (ESI) available: Aniline monomer VMI and further calculation results. See DOI: 10.1039/b000000x/

[a] *J. Heyrovský Institute of Physical Chemistry v.v.i., Czech Academy of Sciences, Dolejškova 3, 18223 Prague, Czech Republic. Fax: +4202 8658 2307; Tel: +4202 6605 3206; E-mail: michal.farnik@jh-inst.cas.cz*
[b] *Institute of Organic Chemistry and Biochemistry v.v.i., Czech Academy of Sciences, Flemingovo nám. 2, 16610 Prague 6, Czech Republic. ; E-mail: dana.nachtigallova@marge.uochb.cas.cz*

Some disagreements exist on the excited state population in the intermediate regime of 269.5 - 240 nm. King et al.[5] claim that at the wavelengths corresponding to the origin of $S_2(3s/\pi\sigma^*)$ state (at the wavelengths $\leq$269.5 nm) the quasi-bound vibrational level along N–H coordinate is populated, while further wavelength lowering results in the excitation into $S_1(1^1\pi\pi^*)$ state followed by an internal conversion to $S_2(^1\pi\sigma^*)$ state. The internal conversion was also attributed to the H-fragment signal observed by Stavros et al. at the wavelengths shorter than 250 nm.[4] Contrary to this, Montero et al.[6] and Fielding et al.[7,8] saw no evidence of S_1 state in photoelectron imaging experiment and predicted a direct S_2 state population. They showed[7,12,13] that at all measured wavelengths (269-238 nm) the $^1\pi\sigma^*$ state is populated directly and it decays by the two different pathways: one via the coupling to the $^1\pi\pi^*$ state through CI in the vFC region with subsequent population transfer to S_0 state, and the second where the population develops on the $^1\pi\sigma^*$ state followed by dissociation or transition to S_0 state. Time-resolved photoelectron imaging of Thompson et al.[9] suggested a simultaneous population of S_1 and S_2 state in the region 273-266 nm and recently confirmed this result also at the wavelength of 250 nm.[11] The most recent discussion of the photoelectron spectra from aniline can be found elsewhere.[12] Although the exact dynamics of the excited aniline is still not determined it is unambiguous that the $^1\pi\sigma^*$ state plays a crucial role providing the fast H-atoms.

The slow statistical H atom channel was also observed experimentally. This channel was detected in a wide range of the excitation wavelengths in H-photofragment imaging experiments resulting in a broad Boltzmann-like component of H-fragment kinetic energy spectra.[4,5] Several processes were suggested to be responsible for these slow H-fragments: (i) fast multiphoton processes, e.g., dissociative ionization producing H^+ directly; (ii) statistical unimolecular decay of vibrationally hot S_0 ground state populated via appropriate CIs. Roberts et al.[4] identified three $1^1\pi\pi^*/S_0$ CIs on the PES and also suggested a possible cascade process via $1^1\pi\pi^*/^1\pi\sigma^*$ and $^1\pi\sigma^*/S_0$ CIs. Although, they have not seen a strong evidence for S_0 repopulation on the time scales shorter than $\sim$100 ps, it can occur at later times.

The important consequences of the $\pi\sigma^*$ state character appear when the heteroaromatic molecule is complexed with other solvating species. Possible reaction channels are available in the excited states including (i) dissociation of hydrogen into free space, (ii) hydrogen transfer between the heterocyclic unit and the solvating molecule, (iii) reaction channel leading to puckered CI, and (iv) coupled electron-proton transfer.[14] The mechanism of the photodissociation process in an isolated molecule depends on the relative energy position of the $\pi\pi^*$ and $\pi\sigma^*$ states which can be influenced by the presence of the solvent.[1] Different effects on the mechanism of the photodissociation via $\pi\sigma^*$ channel were reported for phenol[3,15] and indole[16,17] as compared to pyrrole[18] solvated by ammonia. In the vFC region, these heteroaromatic species exhibit different relative ordering of the $\pi\sigma^*$ and $\pi\pi^*$ states with the $\pi\sigma^*$ located above the $\pi\pi^*$ state for phenole and indole, and below the $\pi\pi^*$ state for pyrrole, respectively.

A combined experimental and computational studies performed on pyrrole and phenol clusters showed that the direct $\pi\sigma^*$ dissociative channel along the N–H coordinate yielding the fast H-fragments was closed. On the contrary, the presence of solvent molecule had a little influence on the valence states resulting from the $\pi \rightarrow \pi^*$ electronic transition.[14,19,20]

Here we focus on aniline clusters and mixed clusters of aniline with water. The aniline dimer and trimer structures were investigated in the ground and excited states previously.[21–23] The N–H site in amino group of aniline can form the hydrogen bond with lone pair of the nitrogen atom of another aniline or with the π electrons of its benzene ring. The neutral structure of the aniline dimer shows relative stability for both conformers: the stacked complexes with N–π type hydrogen bond and N–H$\cdots$N bonding with head-to-tail orientation.[21,22] Analogical structures were found for the trimers.[22]

To reveal the solvent effects on the photochemistry of aniline we vary the size and composition of the complexes from isolated molecules and small $(PhNH_2)_N$, $N \leq 3$, clusters to larger $(PhNH_2)_N$, $N \geq 10$. More about the generation of different aniline clusters in supersonic expansions under various conditions can be found in our recent publication.[24] Water can act as an effective quencher in photochemical reactions and is an important biological solvent. Therefore we investigate also aniline in water clusters from small mixed $PhNH_2{\cdot}(H_2O)_N$, $N \leq 10$, species to $PhNH_2$ molecules deposited on large $(H_2O)_N$, $\bar{N} = 430$ (ice nanoparticles). The structure of neutral aniline-water clusters has not been investigated previously, however, it was studied for cluster ions $[PhNH_2{\cdot}(H_2O)_n]^+$, $n \leq 12$, exhibiting a strong hydrogen bond formation among water molecules with ring-like structure around aniline molecule.[25]

2 Experiment

The present experiments were carried out on two experimental setups: CLUster Beam (CLUB) apparatus and Apparatus for IMaging (AIM). The AIM is a velocity map imaging (VMI) apparatus[26,27] used in the present experiments mainly to confirm the results for isolated molecule. The CLUB is a complex and versatile molecular beam setup specialized in molecular clusters,[27–31] where the photodissociation dynamics and mass spectrometry of different aniline clusters were investigated. The CLUB experiments will be briefly outlined below, further details of the apparatus can be found in our recent publications.[24,28,32,33]

A specially designed temperature controlled nozzle setup with a built in reservoir for solid and liquid samples inside the vacuum chamber was used to generate various aniline species from single molecules to large aniline $(PhNH_2)_N$ clusters and mixed clusters of aniline complexed with water $(PhNH_2)_N{\cdot}(H_2O)_M$. To generate the beam composed mostly of aniline monomers the He carrier gas under 1 bar stagnation pressure passed through the reservoir with aniline at room temperature. Increasing the reservoir temperature and using Ar carrier gas allowed generation of larger clusters. To produce mixed clusters with water, the He gas passed over a $PhNH_2/H_2O$ mixture in ratio 1:5 by volume. To deposit aniline molecules on large water clusters, the pickup technique was used.[34] Pure water clusters $(H_2O)_N$, $\bar{N} \approx 430$, were generated with a different water cluster source[29] and aniline vapour was introduced into a separated pickup chamber by means of an external inlet system with heated aniline sample. The water clusters passing through the pickup cell uptake aniline molecule(s). The neutral $(H_2O)_N$ cluster mean size $\bar{N} \approx 430$ was derived using Bucks' formula.[35,36] Tab. 1 summarizes the expansion conditions.

Table 1 Expansion conditions: stagnation pressure P_0 and reservoir temperature T_R (the nozzle temperature T_0 was higher typically by 10 K). Sizes n denote the largest $(PhNH_2)_n^+$ or $PhNH_2{\cdot}(H_2O)_n^+$ ion fragment discernible in the mass spectra (neutral cluster size $N \geq n$). Nozzle parameters: diameter 50 μm (90 μm for $(H_2O)_N$), opening angle 30°, length 2 mm.

Buffer gas	P_0 (bar)	T_R (K)	Species	Size
He	0.8	303	molecule	
He	2	323-373	$(PhNH_2)_N$	$n \leq 3$
Ar	2-4	323-373	$(PhNH_2)_N$	$n \geq 10$
H_2O/He	2-6	313-343	$PhNH_2{\cdot}(H_2O)_N$	$n \leq 10$
H_2O	4.6	423	$PhNH_2{\cdot}(H_2O)_N$	$\bar{N} \approx 430$

It ought to be mentioned that we use continuous expansions through conical nozzles in the CLUB experiments. This is especially important for the cluster generation, since pulsed nozzles provide different clustering conditions at the different phases of valve opening[26] and often a pulse-to-pulse reproducibility in cluster distribution is poor. On the contrary, the continuous expansions provide very reproducible and stable cluster size distributions which we could verify on CLUB for various clusters by several different mass spectrometric techniques.[29]

The skimmed cluster beam passed through two differentially pumped chambers before entering the chamber hosting the VMI assembly perpendicular to the beam axis. The molecules and clusters interacted with the laser in the center of the electrostatic lens system which extracted the ionic photoproducts towards a position sensitive detector. The original VMI design of Eppink and Parker[37] was used for extraction electrostatic lens. Gating the detector enabled discriminating of other ions apart from H^+. The images were recorded with 16-bit greyscale CCD camera (unibrain Fire-i 780b) with imaging lens (25 mm, f/1.6). The recorded images were analysed using the Hankel reconstruction algorithm.[38] From the integrated radial velocity distributions the final kinetic energy distributions (KEDs) and angular distributions were calculated. The calibration of velocity was achieved through photodissociation of HBr at 243 nm, which produces H-atoms with known velocities.[26]

The H-fragments were photoionized via (2+1) REMPI process at 243.12 nm, and the aniline was photodissociated at the same wavelength in a one-color experiment. The UV laser was scanned over the entire Doppler profile of the resonant transition to record the images. The tunable radiation around 243.1 nm was generated by frequency summing 315 nm with the fundamental 1064 nm of the Nd:YAG laser (Spitlight 1500, Innolas). The tunable 315 nm radiation was produced by doubling a 630 nm output of a dye laser (Pulsare-S, Lioptec) pumped by the second harmonics (532 nm) of the Nd:YAG laser. The lasers were operated at 10 Hz frequency with pulse width 7 ns. The laser radiation was polarized so that the electric field vector of the radiation was parallel to the molecular beam, i.e. perpendicular to the imaging TOF axis.

The photodissociation experiments were accompanied by simultaneous mass spectra measurements using reflectron time-of-flight mass spectrometer (RTOFMS), which provided information about the species in the molecular beam. After the VMI chamber the molecular beam entered the mass spectrometer chamber with RTOFMS mounted perpendicularly to the beam. This mass spectrometer offers several ionization options.[29,36,39,40] In the present study we used electron ionization with an electron gun with 10 kHz repetition frequency and electron energy of 70 eV. The aniline cluster mass spectrometry has been investigated in detail by our recent study where also a more detailed description of our RTOFMS can be found.[24]

3 Theoretical methods

The experiments were complemented by *ab initio* calculations. The ground state equilibrium geometries of aniline molecule and $(PhNH_2)_{2,3}$ clusters were optimized using the density functional method employing the ωB97XD functional which includes empirical dispersion[41] and 6-311G* basis set. The interaction of $PhNH_2$ with the large water cluster (ice nanoparticle) was modelled by the cluster which consist of 50 water molecules. These clusters were taken from the previous ice surface simulation studies as described elsewhere.[42] They were calculated with the B97-D functional[43] and the TZVP basis set.[44] The interaction energies were corrected for basis set superposition error (BSSE). This approach has been suc-

cessfully used for the description of the aromatic species with the ice surface previously.[42]

The calculations of the vertical excitation energies were obtained at the DFT level employing the long-range corrected LC-ωPBE functional[45–47] and aug-cc-pVTZ basis set. The structures at conical intersections on the S_0/S_1 crossing seam have been obtained using SA-CASSCF method.[48–50] To obtain the energetic profiles of all considered stationary points and CI the excitation energies of the resulting geometries were obtained using LC-ωPBE functional. The effectiveness of the CIs were evaluated based on the calculations of linear interpolation curves (LIIC) performed with LC-ωPBE functional. The Gaussian09[51] and Columbus[52] program packages were used to perform the calculations at the DFT and SA-CASSCF levels, respecitively.

4 Experimental results

4.1 Isolated aniline and small aniline clusters

Our measured H-fragment KED from 243 nm aniline molecule photodissociation is in good agreement with the previously reported spectra.[4] Besides, it is essentially identical to the KED obtained for the small aniline clusters shown in Fig. 1 (a) (our isolated molecule KED is shown in the accompanying ESI†). The KED is decoupled into two components: (A) Gaussian peak of fast fragments centered at 0.8 eV originating from the direct N–H bond fission along the $^1\pi\sigma^*$ surface; and a statistical distribution (B) peaking at low energies around 0.1–0.2 eV with a tail extending towards 1.5 eV assigned to the decay of hot S_0 ground state populated through the CI($^1\pi\sigma^*/S_0$).[4,5]

The images were also processed to evaluate the angular distribution of the departing H atom. Integrating the image over the higher kinetic energy region corresponding to the direct dissociation process (A) around 0.8 eV yielded an anisotropy parameter $\beta \approx -0.7 \pm 0.2$ in agreement with the previously reported $\beta = -0.5$.[5] This implies that the excitation is of perpendicular character and the dissociation dynamics is fast compared to the molecular rotation. The anisotropy is apparent from the image in ESI†.

Our main focus is on the photodissociation in clusters. Small aniline clusters were formed already in He expansions at the elevated He-pressure $P_0 = 2$ bar and reservoir temperatures $T_R = 323$–373 K. The mass spectra in Fig. 1 (b) exhibit peaks up to the trimer ion. Due to expected cluster fragmentation upon electron ionization, presumably neutral dimers and trimers are populated significantly in the beam apart from the monomers. The H-fragment signal in the images increased due to the higher particle densities in the beam at the higher T_R. However, the images did not differ significantly from the aniline monomer. The corresponding KED shown in Fig. 1 (a)

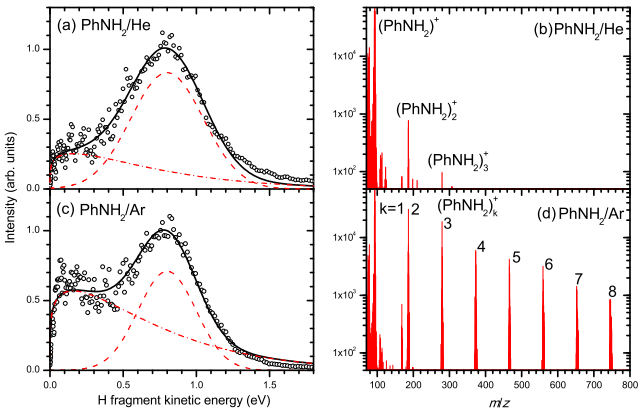

Fig. 1 (a) KED spectrum obtained from the photodissociation of small aniline clusters generated in coexpansion with He at stagnation pressure $P_0 = 2$ bar and reservoir temperature $T_R = 343$ K; the corresponding mass spectrum (b) exhibits ions up to $(PhNH_2)_3^+$. (c) KED spectrum obtained from the photodissociation of larger aniline clusters generated in coexpansion with Ar at stagnation pressure $P_0 = 2$ bar and reservoir temperature $T_R = 323$ K, and the corresponding mass spectrum (d).

is essentially identical with the KED of isolated molecule in ESI†. Thus the photodissociation dynamics in these small clusters (dimers and trimers) is not significantly affected by the solvation.

4.2 Large aniline clusters

To generate a beam dominated by aniline clusters we used Ar as the buffer gas. The mass spectrum in Fig. 1 (d) exhibits aniline cluster ions $(PhNH_2)_n^+$, and clusters larger than $n \geq 10$ are observed. We have shown in our recent detailed mass spectrometric study[24] that under the present conditions pure aniline clusters $(PhNH_2)_N$ were generated. There are some

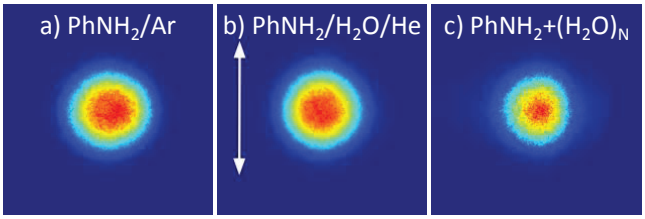

Fig. 2 The H-fragment images from 243 nm photodissociation of aniline clusters generated in $PhNH_2$/Ar expansions (a), $PhNH_2 \cdot (H_2O)_n$ clusters (b), and $PhNH_2$ molecule deposited on large $(H_2O)_N$ clusters (c). The vertical arrow indicates laser polarization.

differences in the H-fragment images from these large aniline clusters, shown in Fig. 2 (a), compared to the images from isolated molecules shown in ESI†. The cluster image is quite

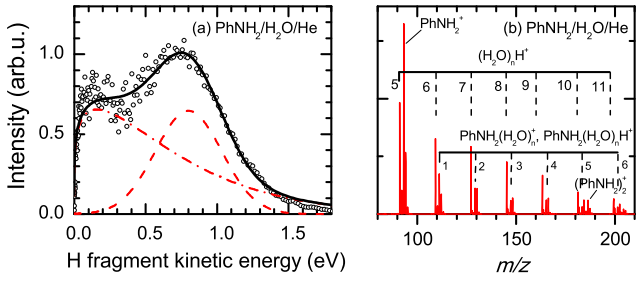

Fig. 3 The KED obtained after photodissociation of aniline-water clusters produced in expansion of $PhNH_2$ and water vapour mixture (1:5 liquid volume ratio) in He $P_0 = 2$ bar and $T_R = 313$ K (a). The corresponding mass spectrum (b).

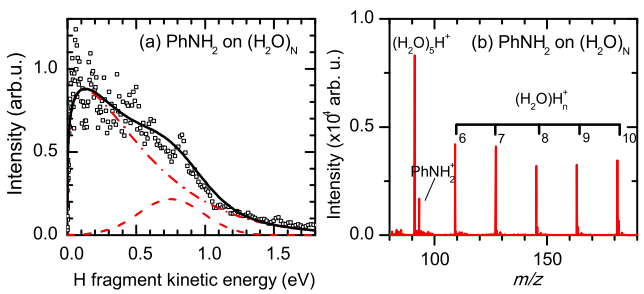

Fig. 4 The KED obtained after photodissociation of aniline picked up on large $(H_2O)_N$, $\bar{N} \approx 430$, clusters produced in pure water vapour expansion $P_0 = 4.6$ bar, $T_R = 423$ K (a). The corresponding TOF mass spectrum (b).

isotropic with $\beta \approx 0$ for the fast fragments (A). This is due to the elastic scattering of the fast H-fragments with the cluster constituents in which they are redirected from their original flight path after the dissociation but do not lose their kinetic energy. Although the H-fragment KED from the larger clusters in Fig. 1 (c) resembles the ones from the isolated molecules and small clusters, Fig. 1 (a), the slow fragment portion is enhanced in the larger clusters significantly. Numerous similar spectra recorded under various conditions with Ar buffer gas confirmed this trend.

4.3 Aniline-water clusters

The mixed species were generated by coexpansion of $PhNH_2$ and water vapour from 1:5 liquid volume mixture in the reservoir. The mass spectrum in Fig. 3 (b) shows several progressions of peaks: $(PhNH_2)_n^+$, $(H_2O)_nH^+$, $PhNH_2{\cdot}(H_2O)_n^+$ and $PhNH_2{\cdot}(H_2O)_nH^+$. The $(H_2O)_nH^+$ ions can originate from pure $(H_2O)_N$ clusters in the beam. However, any significant contribution from the pure water clusters to the present VMI could be excluded since an H signal from pure water clusters at 243 nm can originate only after multiphoton absorption.[53] In the present study the photon flux was kept lower to avoid these multiphoton processes. The processes observed in our previous study[53] of $(H_2O)_N$ were 5-photon processes: 2-photon dissociation and (2+1) H-fragment REMPI. The present processes require essentially 4-photons, since a single-photon dissociation is involved. Therefore, the 5-photon processes could be suppressed at the lower photon fluxes as proved by no H-fragment signal from pure water clusters. Also pure aniline clusters exhibit only a small contribution in the mass spectra. There is a strong monomer $PhNH_2^+$ peak, nevertheless, the image in Fig. 2 (b) and KED in Fig. 3 (a) differ from the isolated molecule: the image is more isotropic, and the KED contains significantly more slow statistical fragments. Thus the H-fragments must originate mostly from the mixed $PhNH_2{\cdot}(H_2O)_N$ clusters. They again exhibit an enhanced slow component (B) compared to the fast one (A).

Finally, we investigated the aniline photodissociation in the extreme case of the individual molecules embedded on the surface of large water clusters $(H_2O)_N$, $\bar{N} \approx 430$. Fig. 4 (b) shows the corresponding mass spectrum with the protonated water peaks and $PhNH_2^+$ peak. This suggests that even in case of multiple molecule pickup, the aniline molecules remain isolated on the water clusters. We have recently observed this lack of coagulation for various molecules deposited on ice nanoparticles.[28,32,34] In this case the KED in Fig. 4 (a) is strongly dominated by the slow statistical component. The fast hydrogen fragments are still present but their fraction is significantly suppressed compared to the aniline and smaller aniline-water clusters.

5 Calculation results

5.1 Isolated aniline

First, we calculate isolated aniline molecule to reference our method to the previously published aniline studies. The results of vertical excitation energies of the three lowest excited states calculated at the TD-LC-ωPBE are compared in ESI† with the previously reported computational results. In comparison to the experimentally observed vertical excitation energy to $1^1\pi\pi^*$ state of 4.4 eV,[54] the calculated absorption energy is overestimated by approximately 0.6 eV, giving a larger error than results obtained with TD-CAM-B3LYP and EOM-CCSD(T).[4] However, we focus here on the clusters, for which the high level calculations are not feasible, and thus the above difference of 0.6 eV provides a rough estimate how the present calculation results can be scaled for a comparison with the experiment.

The optimization of the CI($1^1\pi\sigma^*/S_0$) performed at the MS-CASSCF level resulted in the structure with the N–H bond distances of the corresponding bond fission of 1.832 Å, and this structure was placed 5.06 eV above the energy of the

ground state equilibrium structure. The linear interpolation curves of the PESs of the ground and first three excited states with respect to the N–H bond fission between the vFC region and this CI (shown in ESI†) suggest the previously reported scenario:[4] a direct barrierless path from the $2^1\pi\pi^*$ towards the $1^1\pi\sigma^*/S_0$ CI, leading to the formation of fast hydrogen atoms. The additional paths would include tunneling through the barrier. Based on our results this barrier appeared at the structure with N–H bond distance of 1.337 Å. The wavefunctions of first two excited states were characterized by mixing of $\pi \rightarrow \pi^*$ and $\pi \rightarrow \sigma^*$. Based on the energy values obtained from the linear interpolation curve, this barrier was 0.16 eV above the vertical excitation energy of the $2^1\pi\pi^*$. The optimization of the relevant point with the N–H bond kept fixed resulted in reducing of the energy barrier by 0.20 eV, i.e. below the $2^1\pi\pi^*$ vertical excitation energy and, thus, made a direct reaction channel from $2^1\pi\pi^*$ towards the $1^1\pi\sigma^*/S_0$ CI feasible.

5.2 Aniline dimers

The structure of the two most stable aniline dimer clusters $(PhNH_2)_2$-I and of $(PhNH_2)_2$-II are shown in Fig. 5 (a) and (c), respectively. In the former structure the monomers possess the stacked head-to-tail orientation which is stabilized by hydrogen bonding towards π-aromatic systems, while the latter structure is stabilized by the hydrogen bonding between NH_2 groups. In agreement with previously reported results of *ab initio* calculations[22] the energy difference between these two dimer structures is 1.54 kcal/mol. Note that in the latter structure two types of hydrogen can be identified, those involved in hydrogen bonding and those directed towards a free space. The vertical excitation energies are given in ESI†. The structures of four energetically lowest structures of $PhNH_2$ trimer are also shown in ESI†. These results show that also in the trimers the two types of hydrogen atoms of amino group can be identified, i.e. the ones involved in the hydrogen bonding, and free space pointing hydrogens.

The geometry of $CI(1^1\pi\sigma^*/S_0)$ of $(PhNH_2)_2$-I which corresponds to the hydrogen dissociation is shown in Fig. 5 (b). In this structure the dissociative hydrogen is attached to the aromatic ring of the second molecule. The energy of this CI is, however, 6.46 eV above the ground state minimum structure. This is above the experimental excitation energy. The CI relevant to the hydrogen dissociation in $(PhNH_2)_2$-II dimer is shown in Figs. 5 (d). This structure is characterized by a complex in which the dissociative hydrogen interacts with both nitrogens. Linear interpolation curves (LIIC) between the vFC region and the $CI(1^1\pi\sigma^*/S_0)$ structure is shown in ESI†, Fig. S3. This CI is located 5.81 eV above the ground state minimum and it is, thus, energetically slightly above the experiment (considering the scaling factor between the experiment and calculated results discussed in Sec. 5.1). Taking into account that the description at the DFT level gives only an approximate value due to its multi-configurational character we can assume that this CI is accessed in the current experiment. However, the LIIC connecting the vFC region and this CI is characterized by a barrier of about 6.6 eV. Based on the experience on the constrained optimization of the barrier height on the hydrogen dissociation channel (see Sec. 5.1 and 5.3), lowering of the barrier below the experimental excitation energy is not expected.

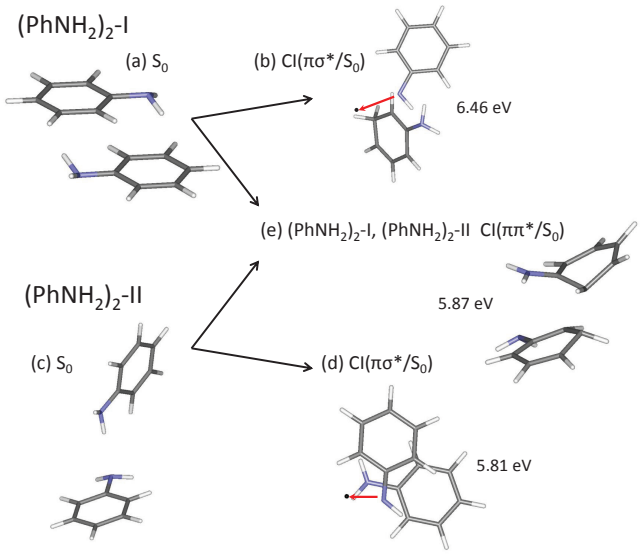

Fig. 5 The optimized aniline dimer structures. Top $(PhNH_2)_2$-I: (a) ground state equilibrium structure of, (b) $CI(1^1\pi\sigma^*/S_0)$. Bottom $(PhNH_2)_2$-II: (c) ground state, (d) $CI(1^1\pi\sigma^*/S_0)$. Middle structure (e) $CI(\pi\pi^*/S_0)$.

Fig. 5 (e) illustrates the CI which can be reached after excitation of both $(PhNH_2)_2$-I and $(PhNH_2)_2$-II dimers. This structure is characterized by a strong distortion of both aromatic rings and it is located energetically 5.87 eV above the ground state minimum. This CI is assumed to be accessible in the current experiment using the same argumentation about the description of CI within the DFT method as given in the previous paragraph . As in the previous case the height of barrier on LIIC was calculated as 6.5 eV. A constrained optimization of the point on LIIC corresponding to the top of the barrier with fixed carbon atoms leads to a lowering of this barrier below the initial excitation energy and, thus, makes this CI effective.

5.3 Aniline-water clusters

To describe the photodissociation in aniline-water clusters two models were considered, Figs. 6 (a) and (d), in which one $(PhNH_2{\cdot}(H_2O)_2$-I) or both $(PhNH_2{\cdot}(H_2O)_2$-II) hydro-

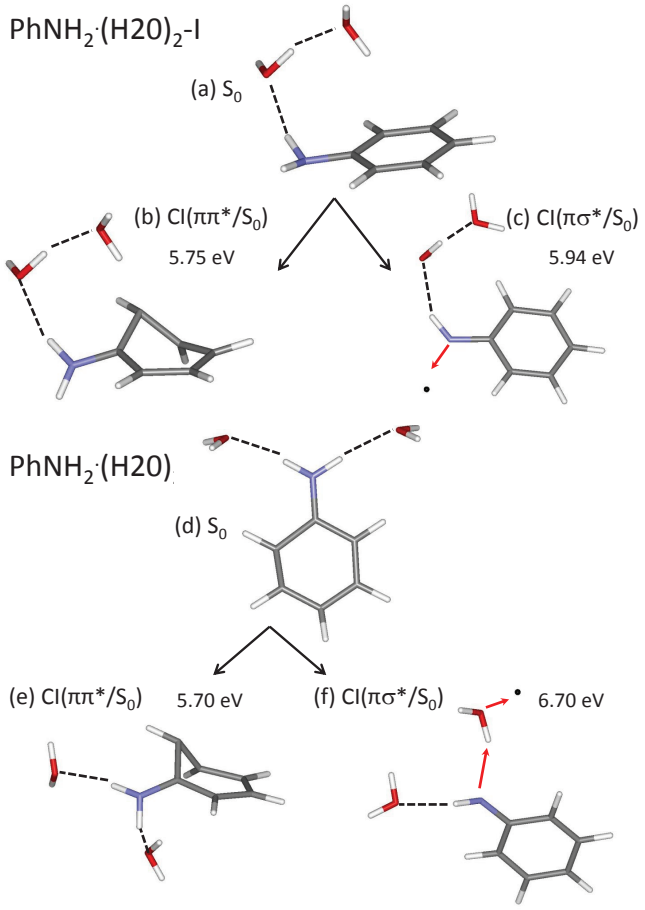

Fig. 6 The optimized structures of $PhNH_2{\cdot}(H_2O)_2$ clusters. Top $PhNH_2{\cdot}(H_2O)_2$-I: (a) ground state, (b) $CI(1^1\pi\pi^*/S_0)$, (c) $CI(1^1\pi\sigma(NH)^*/S_0)$. Bottom $PhNH_2{\cdot}(H_2O)_2$-II: (d) ground state, (e) $CI(1^1\pi\pi^*/S_0)$, (f) $CI(1^1\pi\sigma(OH)^*/S_0)$.

gen atoms of amino group are interacting with the water molecules. The excitation energies in the vFC region are given in ESI†.

The structures of optimized $CI(1^1\pi\pi^*/S_0)$ and $CI(1^1\pi\sigma^*/S_0)$ are shown in Figs. 6 (b) and (c) for $PhNH_2{\cdot}(H_2O)_2$-I, and in Figs. 6 (e) and (f) for $PhNH_2{\cdot}(H_2O)_2$-II, respectively. The character of hydrogen bonding remains unchanged in both excited state minima. The $1^1\pi\pi^*/S_0$ conical intersections are characterized by a distortion of the benzene ring. They are placed by about 5.7 eV above the ground state minima, and thus accessible within our experiment.

The $CI(\pi\sigma^*/S_0)$ in Fig. 6 (c) which corresponds to the dissociation of the hydrogen towards the free space is located energetically slightly above the experimental excitation energy. As in the case of previously described CI we can predict that this CI can be accessible in our experiment, because of the errors due to a single-reference description at the DFT level. Similarly to isolated aniline, the optimization resulted in the planarization of the NH_2 which is accompanied by rearrangement of clustering water molecules. The calculated LIIC between the vFC region and $CI(1^1\pi\sigma^*/S_0)$ calculated for $PhNH_2{\cdot}(H_2O)_2$-I cluster is shown in ESI†, Fig. S5. The barrier on the relevant reaction path is about 0.5 eV higher compared to the experimentally used excitation energy. As in the case of monomer the optimization of the highest point on the potential energy surface leads to the lowering of this barrier by about 0.4 eV making this CI very likely efficient for the hydrogen dissociation. In the $CI(\pi\sigma^*/S_0)$ of $PhNH_2.(H_2O)_2$-II, Fig. 6 (f), the hydrogen dissociating from amino group is attached to the clustering water followed by dissociation of hydrogen from there. This structure is, however, about 1.6 eV above the excitation energy used in the experiment, and thus not accessible for the relaxation process.

Finally, we have calculated the optimized structures of large water clusters with aniline $PhNH_2{\cdot}(H_2O)_{50}$ interacting via a single or both hydrogen bonds formed between the NH_2 group and oxygen atoms of the water molecules. The BSSE corrected interaction energies obtained at the ωB97D functional calculated for these structures are -17.92 kcal/mol and -22.18 kcal/mol, respectively. Thus the double hydrogen bonded structure is more stable by 4.26 kcal/mol. The structures are presented in ESI†.

6 Discussion

6.1 Aniline Clusters

The KEDs of H-fragments from small $(PhNH_2)_N$, $N \leq 3$, clusters closely resemble the spectra of isolated molecules with the fast hydrogens (A) and the slow statistical fragments (B). According to the previous experiments and theoretical calculations for isolated molecules[2,4,5] the excitation at 243 nm should be above the $^1\pi\sigma^*$ transition origin and above the $\pi\pi^*/^1\pi\sigma^*$ CI, and can even reach the $2^1\pi\pi^*$ state. Although the absolute position of these states seems somewhat shifted towards higher energies in our calculations, their relative spacing is in good agreement with the previous experiments.[5,55,56]

Based on the comparison of excitation energies, the first and second pairs of states of $\pi\pi^*$ character of the dimer correspond to the $1^1\pi\pi^*$ and $2^1\pi\pi^*$ states of the monomer, respectively. For both structures, the oscillator strengths of the more intense state corresponding to the monomer $2^1\pi\pi^*$ state is 3-4 times larger than the oscillator strengths of states corresponding to the monomer $1^1\pi\pi^*$ state. Similarly, the transitions to the Rydberg states are less intense, with 15 and 7 times smaller oscillator strengths for the $(PhNH_2)_2$-I and $(PhNH_2)_2$-II, respectively. In this case the dynamics will involve sequential decay through several CIs $2^1\pi\pi^*/1^1\pi\pi^*$, $^1\pi\pi^*/^1\pi\sigma^*$,

and $^1\pi\sigma^*/S_0$. The previous experimental measurements of the time constant for H atom elimination at $\lambda \leq 240$ nm showed very fast dynamics with $\tau \approx 155$ fs proving very efficient population transfer from $2^1\pi\pi^*$ to $^1\pi\sigma^*$ state.[4] This dynamics yields the fast (A) fragments. The slow fragments (B) were also observed in a wide range of the excitation wavelengths[4,5] generated by a statistical decay of the hot ground state S_0 populated via available CIs ($^1\pi\sigma^*/S_0$, $^1\pi\pi^*/S_0$).

In the larger clusters (generated in Ar expansions), the slow contribution increases. This observation is similar to the case of pyrrole, pyrazole, imidazole, and phenol studied in clusters previously.[14,19,20,57–59] The pathway along the hydrogen bonding N–H coordinate towards the $^1\pi\sigma^*/S_0$ CI and thus towards the fast channel closes by complexation in clusters. However, in the case of aniline there are two N–H bonds and, if the other one remains free, it can still be dissociated. Thus in aniline the cluster effect is not as pronounced as in the case of the molecule with a single N–H bond and sets on for the larger clusters.

It is worth noting, that our one-color experiment probes only the H-fragments generated withing the time window of a single laser pulse of ≈7 ns. The slow H-atoms born through statistical decay are likely to continue to form beyond this time-window. Thus the fast fragment peak A might be somewhat enhanced with respect to the slow peak B in the present spectra. Similar effect is evident in the differences between the kinetic energy spectra from Rydberg-tagging TOF[5] and time-resolved VMI[4] at 240 nm. This can be especially true in the clusters where the dynamics of statistical decay can be significantly slowed down, as we have demonstrated previously for acetylene clusters.[60]

As discussed above, our calculations revealed that in dimers there are two types of hydrogen atoms in amino group, those directed into a free space and those involved in the hydrogen bonding. The former type of hydrogens exists in the optimized ground state and S_1 minimum structures, as well as $\pi\sigma^*/S_0$ CI of $(PhNH_2)_2$-II, Fig. 5 (c) and (d). The latter type of hydrogen atoms correspond to those bound either by interaction with π system or with the amino group of the surrounding molecule in the cluster, as found for $(PhNH_2)_2$-I and $(PhNH_2)_2$-II, Fig. 5.

The free N–H bonds resemble the monomer behaviour, i.e. they provide both fast and slow H-fragments. The prevailing fast ones result from a direct dissociation. The slow hydrogens result from the statistical decay of the vibrationally hot S_0 ground state populated via $\pi\pi^*/S_0$ and $\pi\sigma^*/S_0$ CIs. Indeed such CIs were found in our calculations for the dimer, and were energetically available with our excitation energy. On the other hand, the hydrogen bonding blocks the dissociative channels and, thus, the hydrogens from the N–H bonds engaged in the hydrogen bonding cannot contribute to the formation of the fast fragments, but they may be funnelled via available CIs into the population of the slow statistical ones.

Our calculated trimer structures (see ESI† Fig. S4) resemble the bonding motives discussed here for the dimers. Therefore we expect similar photochemical behaviour also in small aniline clusters beyond the dimers. Presumably, in significantly larger clusters the number of free N–H bonds decreases with respect to the ones engaged in the hydrogen bonding, and thus the fast fragments decrease relative to the slow ones.

Since our experiment is not completely size-selective and a certain cluster size distribution determined by expansion conditions is generated in the beam, we cannot exclude the presence of isolated monomers even in the beam of larger clusters. Therefore an alternative explanation of our experimental results can be that the fast fragments stem from the isolated monomers. However, two experimental observations suggest that this is not the case entirely: the image isotropy and the mass spectra. The images from large clusters were isotropic, Fig. 2 (a), with the anisotropy parameter $\beta \approx 0$ integrated over the fast fragment region around 0.8 eV. This suggests that the fast H-fragments undergo elastic collisions within the cluster and are scattered isotropically upon leaving the clusters. Such behaviour was observed previously upon photodissociation in clusters.[61,62] In the present case the fast fragments strongly overlap with the slow ones distributed isotropically. Yet, since the isolated molecule photodissociation anisotropy is relatively large $\beta \approx$ -0.7, at least some anisotropy would be preserved if the fast H-fragments would originate entirely from the isolated molecules in the beam. Also the relatively large ion fragments $(PhNH_2)_n^+$ with $n \geq 10$ in the mass spectra suggest significantly larger neutral precursors with log-normal distribution.[29] Therefore the monomer contribution is not expected to prevail in the beam. Even though these observations suggest that the fast fragments do not originate only from the monomers in the beam, this possibility cannot be disproved unambiguously and is left opened as a possible - although less likely - interpretation of our present results.

In addition, some of the slow fragments may originate from the fragmentation of the ionic clusters generated in multiphoton ionization of aniline clusters. We have tried to avoid this contribution in our experiment by lowering the photon flux as outlined in ESI†. The VMI experiments were performed under the conditions where no aniline cluster ion signal from direct multiphoton ionization was observed. This suggests that the H^+ contribution from direct multiphoton ionization of aniline clusters was not overwhelming.

6.2 Mixed clusters with water

The VMI images and KEDs corresponding to the small mixed clusters resemble closely the pure large aniline clusters. According to the mass spectra, here the contribution from isolated molecules in the beam can be more significant than in the case of large aniline cluster discussed above. There-

fore the fast H-atoms could still originate from the photodissociation of the isolated molecules. However, in this case we would expect the anisotropy observed for the isolated molecule photodissociation as discussed above. Again, the images exhibit isotropic distribution with $\beta \approx 0$ for the fast fragments suggesting that they originate mostly from the clusters. The mass spectra also demonstrate that there are no large pure $(PhNH_2)_N$ clusters generated in the $PhNH_2$:H_2O/He expansions. Thus the fast H-fragments arise from the mixed $PhNH_2 \cdot (H_2O)_N$ clusters.

Similarly to aniline clusters, solvation of aniline by water can lead to the formation of clusters in which only one or both hydrogen atoms of NH_2 group are involved in hydrogen bonds with water molecules, Fig. 6. In the former case the calculations predict an existence of a direct dissociation along the free N–H bond leading to the fast and slow H fragments with the same relaxation mechanisms as was suggested for isolated aniline. This situation can be applied to structural motifs observed in $PhNH_2 \cdot (H_2O)_2$-I. In the second type, $PhNH_2 \cdot (H_2O)_2$-II, only the bonded hydrogen atoms are available. The evaluation of the relative energies of CI shows that these bonding motifs block the direct dissociation pathways.

When the aniline molecule is deposited on a large $(H_2O)_N$ cluster, we observe quite a decrease of the fast H-fragments compared to the slow statistical ones. This can be explained if the structures with two hydrogen bonds dominate among the $PhNH_2 \cdot (H_2O)_N$ clusters over the single-bond structures (see Fig. S6 in ESI†). The former structures are by 4.26 kcal/mol more stable than the latter ones. The water cluster temperature on which the aniline is adsorbed in the molecular beam is about 100 K.[63] Thus it is reasonable to assume that the more stable structure will be stabilized on the cluster. Anchoring the molecules with two N–H bonds pointing towards the cluster surface will efficiently close the direct $\pi\sigma^*$ dissociation channel.

Finally, it worth noting, that no strong zero-kinetic-energy peak was observed from the large clusters (neither from the large pure aniline clusters nor from aniline deposited on the ice nanoparticles). Usually a very narrow and pronounced maxima in VMI images and KEDs provide evidence for fragment *caging* in clusters[61,62,64,65] as observed, e.g., in photodissociation of hydrogen halides[26,28] and freons[27,32] on/in Ar clusters, or most recently in photodissociation of ethanethiol clusters.[33] We have also demonstrated that this narrow maximum should not be confused with a "central blob" of slow fragments in images which can point to quite different dynamics.[28,33] Thus in the present case, there is no *caging* (in Bucks' sense[64]) of the H-fragments in the aniline clusters. Either, the clusters are not large enough to slow down the H-fragments to zero kinetic energy, although the mass spectra show evidence for clusters with more than 10 molecules, or the fragment caging is inefficient in these clusters. On the other hand, the isotropic distribution in the fast H fragments demonstrates the elastic collisions of leaving hydrogens with the cluster constituents.

7 Conclusions

We have investigated the 243 nm photodissociation dynamics of N–H bond in aniline in different complex cluster environments: from isolated molecules to small $(PhNH_2)_N$, $N \leq 3$, and larger $(PhNH_2)_N$, $N \geq 10$, clusters, and from small mixed $PhNH_2 \cdot (H_2O)_N$, $N \leq 10$, clusters to individual $PhNH_2$ molecules deposited on large $(H_2O)_N$, $\bar{N} = 430$, clusters. The main conclusions of the complementary experimental and theoretical investigations can be summarized as follows:

- For isolated aniline molecules we have confirmed the previous experimental and theoretical results and supported the proposed dynamical scenarios for the fast and slow H-fragment generation by further theoretical investigations.
- Small clusters $(PhNH_2)_N$, $N \leq 3$, exhibit very similar behavior to the isolated molecules mainly due to the presence of the free N–H bonds in these clusters.
- Large clusters $(PhNH_2)_N$, $N \geq 10$, exhibit increasing contribution of slow statistical fragments compared to the fast ones. This is rationalized based on our calculations by closing the direct N–H dissociation channel. This closing drives the population towards other coordinates which eventually funnel the population through available CIs onto the hot ground state decaying statistically.
- Small mixed $PhNH_2 \cdot (H_2O)_N$, $N \leq 10$, clusters show similar behavior with the increased contribution of slow statistical fragments. Our calculations support similar scenario as above, closing of the direct N–H dissociation channel. The calculations show also free N–H bonds in the $PhNH_2 \cdot (H_2O)_N$ clusters which yield the fast fragment contribution. Based on the relative energies of the relevant CI we predict that the generation of slow statistical fragments is slightly preferred.
- The individual $PhNH_2$ molecules dissociated on a surface of ice nanoparticles yield the slow fragments almost exclusively, which the calculations rationalize by a more stable structure of $PhNH_2 \cdot (H_2O)_{50}$ cluster with two hydrogen bonds, thus closing the direct dissociation pathways for both N–H bonds.

The general pattern observed not only here but also in our previous investigations of heteroaromatic molecule photodissociation in clusters[14,19,20,59] can be formulated intuitively: the engagement of the dissociation N–H bond into the hydrogen bonding with solvating molecules closes the direct dissociation along the repulsive $\pi\sigma^*$ potential yielding the fast

hydrogen fragments and funnels the population into the slow hydrogens from a statistical decay of vibrationally hot ground state instead. However, the present combination of VMI experiment and *ab initio* calculations offers a more detailed insight into the influence of the solvent - water molecules, in particular - on the photodissociation dynamics of the N–H bond in aniline, illustrating the complexity of the solvent effects even in this relatively simple system.

Acknowledgment: This work was supported by the Czech Science Foundation project No.: 14-14082S.

References

1 M. N. R. Ashfold, B. Cronin, A. L. Devine, R. N. Dixon and M. G. D. Nix, *Science*, 2006, **312**, 1637.
2 G. M. Roberts and V. G. Stavros, *Chem. Sci.*, 2014, **5**, 1698 – 1722.
3 A. Sobolewski, W. Domcke, C. Dedonder-Lardeux and C. Jouvet, *Phys. Chem. Chem. Phys.*, 2002, **4**, 1093.
4 G. M. Roberts, C. A. Williams, J. D. Young, S. Ullrich, M. J. Patterson and V. G. Stavros, *J. Am. Chem. Soc.*, 2012, **134**, 12578 – 12589.
5 G. A. King, T. A. A. Oliver and M. N. R. Ashfold, *J. Chem. Phys.*, 2010, **132**, 214307.
6 R. Montero, A. P. Conde, V. Ovejas, R. Martínez, F. Castaño and A. Longarte, *J. Chem. Phys.*, 2011, **135**, 054308.
7 R. Spesyvtsev, O. M. Kirkby and H. H. Fielding, 2012, **157**, 165 – 179.
8 R. Spesyvtsev, O. M. Kirkby, M. Vacher and H. H. Fielding, *Phys. Chem. Chem. Phys.*, 2012, **14**, 9942 – 9947.
9 J. O. F. Thompson, R. A. Livingstone and D. Townsend, *J. Chem. Phys.*, 2013, **139**, 034316.
10 F. Wang, S. P. Neville, R. Wang and G. A. Worth, *J. Phys. Chem. A*, 2013, **117**, 7298.
11 J. O. F. Thompson, L. Saalbach, S. W. Crane, M. J. Paterson and D. Townsend, *J. Chem. Phys.*, 2015, **142**, 114309.
12 O. M. Kirkby, M. Sala, G. Balerdi, R. de Nalda, L. Bañares, S. Guérin and H. H. Fielding, *Phys. Chem. Chem. Phys.*, 2015, **17**, 16270 – 16276.
13 M. Sala, O. M. Kirkby, S. Guérin and H. H. Fielding, *Phys. Chem. Chem. Phys.*, 2014, **16**, 3122.
14 P. Slavíček and M. Fárník, *Phys. Chem. Chem. Phys.*, 2011, **13**, 12123.
15 G. Pino, A. N. Oldani, E. Marceca, M. Fujii, S.-I. Ischiuchi, M. Miyazaki, M. Broquier, C. Dedonder and C. Jouvet, *J. Chem. Phys.*, 2010, **133**, 124313.
16 H. Lippert, V. Stert, C. P. Schulz, I. V. Hertel and W. Radloff, *Phys. Chem. Chem. Phys.*, 2004, **6**, 2718.
17 A. L. Sobolewski and W. G. Domcke, *J. Phys. Chem. A*, 2007, **111**, 11725.
18 L. Rubio-Lago, G. A. Amaral, A. N. Oldani, J. D. Rodríguez, M. G. Gonzáles, G. A. Pino and L. Bañares, *Phys. Chem. Chem. Phys.*, 2011, **13**, 1082.
19 V. Poterya, V. Profant, M. Fárník, P. Slavíček and U. Buck, *J. Chem. Phys.*, 2007, **127**, 064307.
20 V. Poterya, L. Šištík, P. Slavíček and M. Fárník, *Phys. Chem. Chem. Phys.*, 2012, **14**, 8936 – 8944.
21 J. H. Yeh, T. L. Shen, D. G. Nocera, G. E. Leroi, I. Suzuka, H. Ozawa and Y. Namuta, *J. Phys. Chem.*, 1996, **100**, 4385 – 4389.
22 D. Schemmel and M. Schütz, *J. Chem. Phys.*, 2010, **132**, 174303.
23 D. Schemmel and M. Schütz, *J. Chem. Phys.*, 2010, **133**, 134307.
24 J. Lengyel, V. Poterya and M. Fárník, *J. Mass. Spectrom.*, 2015, **50**, 643 – 649.
25 M. Alauddin, J. K. Song and S. M. Park, *Int. J. Mass Spectrom.*, 2012, **314**, 49 – 56.
26 J. Fedor, J. Kočišek, V. Poterya, O. Votava, A. Pysanenko, L. Lipciuc, T. N. Kitsopoulos and M. Fárník, *J. Chem. Phys.*, 2011, **134**, 154303.
27 V. Poterya, J. Kočišek, A. Pysanenko and M. Fárník, *Phys. Chem. Chem. Phys.*, 2014, **16**, 421 – 429.
28 V. Poterya, J. Lengyel, A. Pysanenko, P. Svrčková and M. Fárník, *J. Chem. Phys.*, 2014, **141**, 074309.
29 J. Lengyel, A. Pysanenko, V. Poterya, J. Kočišek and M. Fárník, *Chem. Phys. Lett.*, 2014, **612**, 256 – 261.
30 J. Lengyel, A. Pysanenko, V. Poterya, P. Slavíček, M. Fárník, J. Kočišek and J. Fedor, *Phys. Rev. Lett.*, 2014, **112**, 113401.
31 M. Fárník and V. Poterya, *Front. Chem.*, 2014, **2**, 4.
32 V. Poterya, J. Kočišek, J. Lengyel, P. Svrčková, A. Pysanenko, D. Hollas, P. Slavíček and M. Fárník, *J. Phys. Chem. A*, 2014, **118**, 4740 – 4749.
33 P. Svrčková, A. Pysanenko, J. Lengyel, P. Rubovič, J. Kočišek, V. Poterya, P. Slavíček and M. Fárník, *Phys. Chem. Chem. Phys.*, 2015, DOI: 10.1039/c5cp00367a.
34 A. Pysanenko, A. Habartová, P. Svrčková, J. Lengyel, V. Poterya, M. Roeselová, J. Fedor and M. Fárník, *J. Phys. Chem. A*, 2015, DOI: 10.1021/acs.jpca.5b05368.
35 C. Bobbert, S. Schütte, C. Steinbach and U. Buck, *Eur. Phys. J. D*, 2002, **19**, 183–192.
36 J. Kočišek, J. Lengyel, M. Fárník and P. Slavíček, *J. Chem. Phys.*, 2013, **139**, 214308.
37 A. T. J. B. Eppink and D. H. Parker, *Rev. Sci. Instrum.*, 1997, **68**, 3477.
38 B. Whitaker, *Imaging in Molecular Dynamics*, Cambridge University Press, Cambridge, 2003.
39 J. Kočišek, J. Lengyel and M. Fárník, *J. Chem. Phys.*, 2013, **138**, 124306.
40 J. Lengyel, R. Gorejová, Z. Herman and M. Fárník, *J. Phys. Chem. A*, 2013, **117**, 11225 – 11232.
41 J.-D. Chai and M. Head-Gordon, *Phys. Chem. Chem. Phys.*, 2008, **10**, 6615 – 20.
42 D. Heger, D. Nachtigallová, F. Surman, J. Krausko, B. Magyarová, M. Brumovský, M. Rubeš, I. Gladich and P. Klán, *J. Phys. Chem. A*, 2011, **115**, 11412 – 11422.
43 S. Grimme, *J. Comput. Chem.*, 2006, **27**, 1787–1799.
44 A. Schäfer, C. Huber and R. Ahlrichs, *J. Chem. Phys.*, 1994, **100**, 5829.
45 O. A. Vydrov and G. E. Scuseria, *J. Chem. Phys.*, 2006, **125**, 234109.
46 O. A. Vydrov, J. Heyd, A. Krukau and G. E. Scuseria, *J. Chem. Phys.*, 2006, **125**, 074106.
47 O. A. Vydrov, G. E. Scuseria and J. P. Perdew, *J. Chem. Phys.*, 2007, **126**, 154109.
48 H. Lischka, M. Dallos and R. Shepard, *Mol. Phys.*, 2004, **100**, 1647.
49 H. Lischka, M. Dallos, P. G. Szalay, D. R. Yarkony and R. Shepard, *J. Chem. Phys.*, 2004, **120**, 7322.
50 M. Dallos, H. Lischka, R. Shepard, D. R. Yarkony and P. G. Szalay, *J. Chem. Phys.*, 2004, **120**, 7330.
51 M. J. Frisch, G. W. Trucks, H. B. Schlegel, G. E. Scuseria, M. A. Robb, J. R. Cheeseman, G. Scalmani, V. Barone, B. Mennucci, G. A. Petersson, H. Nakatsuji, M. Caricato, X. Li, H. P. Hratchian, A. F. Izmaylov, J. Bloino, G. Zheng, J. L. Sonnenberg, M. Hada, M. Ehara, K. Toyota, R. Fukuda, J. Hasegawa, M. Ishida, T. Nakajima, Y. Honda, O. Kitao, H. Nakai, T. Vreven, J. A. Montgomery, Jr., J. E. Peralta, F. Ogliaro, M. Bearpark, J. J. Heyd, E. Brothers, K. N. Kudin, V. N. Staroverov, R. Kobayashi, J. Normand, K. Raghavachari, A. Rendell, J. C. Burant, S. S. Iyengar, J. Tomasi, M. Cossi, N. Rega, J. M. Millam, M. Klene, J. E. Knox, J. B. Cross, V. Bakken, C. Adamo, J. Jaramillo, R. Gomperts, R. E. Stratmann, O. Yazyev, A. J. Austin, R. Cammi, C. Pomelli, J. W. Ochterski, R. L. Martin, K. Morokuma, V. G. Zakrzewski, G. A. Voth, P. Salvador, J. J. Dannenberg, S. Dapprich, A. D. Daniels, O. Farkas, J. B. Foresman, J. V. Ortiz, J. Cioslowski and D. J. Fox, *Gaussian 09 Revision D*, Gaussian Inc. Wallingford CT 2009.
52 H. Lischka, R. Shepard, I. Shavitt, R. M. Pitzer, M. Dallos, T. Mller, P. G. Szalay, F. B. Brown, R. Ahlrichs, H. J. Bhm, A. Chang, D. C.

Comeau, R. Gdanitz, H. Dachsel, C. Ehrhardt, M. Ernzerhof, P. Hchtl, S. Irle, G. Kedziora, T. Kovar, V. Parasuk, M. J. M. Pepper, P. Scharf, H. Schiffer, M. Schindler, M. Schler, M. Seth, E. A. Stahlberg, J.-G. Zhao, S. Yabushita, Z. Zhang, M. Barbatti, S. Matsika, M. Schuurmann, D. R. Yarkony, S. R. Brozell, E. V. Beck, , J.-P. Blaudeau, M. Ruckenbauer, B. Sellner, F. Plasser and J. J. Szymczak, *COLUMBUS*, an ab initio electronic structure program, release 7.0 (2012).

53 V. Poterya, M. Fárník, M. Ončák and P. Slavíček, *Phys. Chem. Chem. Phys.*, 2008, **10**, 4835.

54 K. Kimura and S. Nafakura, *Mol. Phys.*, 1965, **9**, 117.

55 W. E. Sinclair and D. W. Pratt, *J. Chem. Phys.*, 1996, **105**, 7942.

56 T. Ebata, C. Minejima and N. Mikami, *J. Phys. Chem. A*, 2002, **106**, 11070.

57 L. Rubio-Lago, D. Zaouris, Y. Sakellariou, D. Sofikitis, T. N. Kitsopoulos, F. Wang, X. Yang, B. Cronin, A. L. Devine, G. A. King, M. G. D. Nix and M. N. R. Ashfold, *J. Chem. Phys.*, 2007, **127**, 064306.

58 M. L. Lipciuc, F. Wang, X. Yang, T. N. Kitsopoulos, G. S. Fanourgakis and S. S. Xantheas, *Chem. Phys. Chem.*, 2008, **9**, 1838.

59 V. Poterya, V. Profant, M. Fárník, L. Šištík, P. Slavíček and U. Buck, *J. Phys. Chem. A*, 2009, **113**, 14583.

60 M. Fárník, V. Poterya, O. Votava, M. Ončák, P. Slavíček, I. Dauster and U. Buck, *J. Phys. Chem. A*, 2009, **113**, 7322.

61 P. Slavíček, P. Jungwirth, M. Lewerenz, N. H. Nahler, M. Fárník and U. Buck, *J. Chem. Phys.*, 2004, **120**, 4498.

62 M. Fárník, N. H. Nahler, U. Buck, P. Slavíček and P. Jungwirth, *Chem. Phys.*, 2005, **315**, 161.

63 N. Gimelshein, S. Gimelshein, C. C. Pradzynski, T. Zeuch and U. Buck, *J. Chem. Phys.*, 2015, **142**, 244305.

64 U. Buck, *J. Phys. Chem. A*, 2002, **106**, 10049.

65 N. H. Nahler, M. Fárník, U. Buck, H. Vach and R. B. Gerber, *J. Chem. Phys.*, 2004, **121**, 1293.